Inertial nonlinear equilibration of equatorial flows

By BACH LIEN HUA[1], DENNIS W. MOORE[2] †
AND SYLVIE LE GENTIL[1]

[1] Laboratoire de Physique des Oceans, IFREMER, BP 70, 29280 Plouzané, France
[2] JIMAR, University of Hawaii, Honolulu, HI 96822, USA

We explore the nature of inertial equilibration of equatorial flows in the presence of mean meridional and vertical shears of the basic state, with oceanic applications in mind. The study is motivated by the observational evidence that the subthermocline equatorial mean circulation displays nearly zero Ertel potential vorticity away from the equator, when taking into account the non-traditional horizontal component of the Earth rotation. This observed state precisely verifies the marginal condition for inertial instability: a linear analysis for the equatorial β-plane confirms that the usual condition of instability, namely that Ertel potential vorticity should be of opposite sign to the vertical Coriolis parameter, remains valid even when the traditional approximation is relaxed. Analytical linear normal modes reveal that a meridional shear of the basic state leads to a vertical stacking of equatorially-trapped zonal flows of alternate signs, with a new centre of symmetry located at the dynamical equator. A vertical shear of the basic state causes a meridional stacking of extra-equatorial zonal flows.

In an inviscid framework, a two-dimensional formulation is ill-posed and we resort to non-hydrostatic viscous simulations to determine the nonlinear normal forms of the system. The influence of a small-scale eddy diffusivity and a large-scale Rayleigh damping on the equilibrated vertical scale is determined numerically. The nonlinear equilibration occurs through a steady-state bifurcation from a basic state without jets to another steady state with secondary jets of alternate signs. The final state corresponds to eastward jets located on the geographic equator, while westward jets are located near the dynamical equator. These results are consistent with *in situ* observations of equatorial deep jets.

The analogy between the equatorial meridional shear flow and the cylindrical Couette–Taylor flow with an axial density stratification is detailed. There is a strong similarity in the general symmetries and nonlinear normal forms of the two problems. Similarly to the homogeneous Couette–Taylor flow, the gap width between the two cylinders is important for determining the axial scale of the secondary flow through the Reynolds number. For the equatorial problem, an upper bound for the height scale of inertial jets is such that the corresponding equatorial radius of deformation times $\sqrt{2}$ fits between the geographic and dynamic equators.

One of our main conclusions is that the *raison d'être* of the observed region of zero Ertel potential vorticity is to facilitate angular momentum exchanges between the two hemispheres and inertial deep jets are the byproducts of this angular momentum mixing.

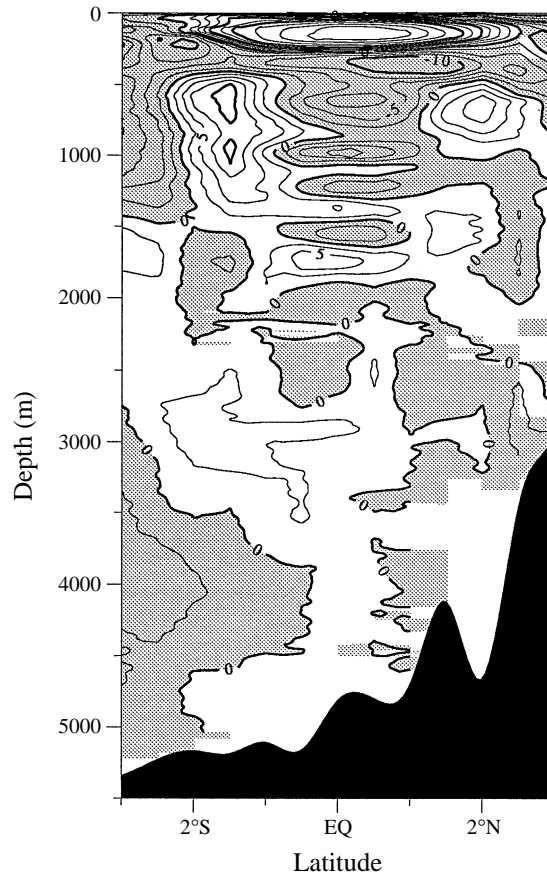† Present address: PMEL, 7600 Sand Point Way, Seattle, WA 98115, USA.

FIGURE 1. Time-mean zonal velocity in the Central Pacific resulting from an 18 month average (February 1982–June 1983) from the PEQUOD data set (from Firing 1987).

1. Introduction

It is now recognized that the occurrence of symmetric instability in the atmosphere (Emanuel 1988) is often observed in regions of near neutrality to inertial instability, for which the Ertel potential vorticity of the flow is zero (Hoskins 1974). This zero-Ertel-potential vorticity state precisely corresponds to the observed mean state of oceanic equatorial flows in wide regions below the thermocline, as will be demonstrated below. This observation has motivated the present systematic study of equatorial inertial instability which is triggered by both vertical and latitudinal shears. The aim is to find a rationale for the geometry of the deep zonal jets which are observed in the equatorial subthermocline mean flow, well beneath the eastward undercurrent which lies at about 200 m depth (figure 1, taken from Firing 1987). One system of zonal jets which are located between 300 and 1800 m, the so-called equatorial deep jets, has a slight meridional offset but is strongly trapped within 1° of the equator, and presents a very small aspect ratio of vertical to horizontal scales. Another set of jets reaches its maximum away from the equator at about 1.5°, has larger vertical scales, and displays a high degree of symmetry about the equatorial plane. What is striking in figure 1 is the stacking of zonal flows of alternate signs in both the vertical and meridional directions. Such a structure of the mean flow, with alternate-signed

jets which appear to be intrinsic parts of the time-mean state, raises the questions (i) what is the mechanism of the jets formation and (ii) how do they equilibrate at finite-amplitude? Equatorial deep jets are a ubiquituous feature of the circulation in all three oceans, since their original discovery by Luyten & Swallow (1976) in the western Indian ocean. A simple explanation has been given in the literature in terms of surface-forced vertically propagating linear waves (Wunsch 1977; McCreary 1984; McCreary & Lukas 1986), but it is difficult to get energy at low frequencies and high vertical wavenumbers to penetrate to great depth because of reflections from the thermocline (Gent & Luyten, 1985) and of the inherent small vertical group velocities. Overall, observations of a systematic and coherent vertical shift of the deep jets have remained elusive, and the propagation issue still lacks convincing evidence (Ponte & Luyten 1989). Most theoretical studies (references cited above; Eriksen 1981; Ponte 1988) have relied on linear equatorial wave ideas. On the other hand, Kawase (1987) and Wang, Moore & Rothstein (1994) explored the possibility that the deep jets are forced by deep western boundary currents, but their solutions are transient, and the issue of the equilibration of time-mean structures could not be addressed, as was the case for the studies which invoked vertical propagation effects.

In contrast, the process which is put forward in the present work is based on a cellular inertial instability mechanism, which is local and a propagation mechanism from a distant energy source is not required. Inertial instability corresponds to the occurrence, within a rotating frame of reference, of what is more generally known as centrifugal instability, when an initially adverse distribution of angular momentum triggers the onset of secondary flows which act to redistribute angular momentum (Rayleigh 1916). This instability can be experimentally realized in a set-up of two concentric cylinders which can rotate independently (Taylor 1923), in particular when the inner cylinder reaches a critical speed while the outer one is maintained fixed. For unstable conditions the azimuthal Couette flow is replaced by cellular patterns in which the fluid travels in helical paths around the cylinders in layers of vortices – now known as Taylor vortices. The corresponding fluid dynamics problem is referred to as the Couette–Taylor problem, and it has become in recent years a paradigm for exploring the complexity of hydrodynamical instability and pattern formation. Recent monographs on the topic are Chossat & Ioss (1994), which deals with the problem from the mathematical point of view of bifurcation theory and symmetry, while Koshmieder (1993) puts more emphasis on laboratory experiments. A general overview of recent research is given in Tagg (1994), and it may be a useful introduction to the nearly 2000 papers connected with the Couette–Taylor problem. Yet among these works, very few have addressed the case of a stable, axial stratification in density, which is the relevant configuration for geophysical applications. We shall prove in the present paper that there is a close analogy between the equatorial inertial instability problem with latitudinal shear and the Couette–Taylor problem in the presence of an axial density stratification. This motivated Boubnov, Gledzer & Hopfinger (1995) and Boubnov *et al.* (1996) to perform laboratory experiments for the stratified case, and their results have been reproduced in the direct numerical experiments of Hua, Le Gentil & Orlandi (1996). The main effect of a density stratification is to reduce the height of the axisymmetric Taylor vortices and to cause the formation of density layers of small aspect ratio. The first flow transition is clearly axisymmetric and is stationary for a Prandtl number of 1. Further flow transitions, which are obtained at larger speeds of the inner cylinder, correspond to larger aspect ratios of the density layers, can have an oscillatory temporal behaviour and can become three-dimensional.

For both the atmosphere and ocean, equatorial regions correspond to the location of

the maximum angular momentum of the fluid and small deviations in the symmetries of the flow are likely to trigger centrifugal instabilities. Symmetry breaking is immediately induced by the existence of a non-zero latitudinal shear at the equator and low-latitude regions are thus privileged locations for the occurrence of inertial instability. This may explain why structures which bear some resemblance to the equatorial deep jets have also been observed in the equatorial middle atmosphere through satellite observations (Hitchman *et al.* 1987). That work first documents the occurrence of planetary-scale disturbances in the equatorial lower mesosphere, which consist of vertically stacked temperature extrema of alternating sign, persist for as long as two weeks and do not propagate. Their very small vertical-to-meridional aspect ratio has led to their labelling as 'pancake structures' and their occurrence is confined to regions of very weak or negative inertial stability. The recent observational study by Knox (1996), which is based on the more comprehensive Upper Atmosphere Research Satellite data set, further supports the above interpretation. Near the solstices, regions of anomalous potential vorticity (PV) tend to develop negative PV in the northern hemisphere in December, positive PV in the southern hemisphere in June, and small aspect ratio layered structures are confined in the equatorial upper stratosphere/lower mesosphere areas.

Among the theoretical studies on inertial instability in the equatorial atmosphere, authors like Boyd & Christidis (1982), Stevens (1983) and Dunkerton (1981, 1983) have focused upon the linear effects of latitudinal shear, while Zhao & Ghil (1991) have addressed the nonlinear inertial instability of both latitudinal and vertical shears in a two-layer formulation for an *a priori* dominance of low vertical modes. For the most part however, conceptual developments of inertial instability dynamics have been obtained in the context of atmospheric conditional (moist) symmetric instability, as first proposed by Bennetts & Hoskins (1979). An extensive treatment of the topic can be found in the book by Emanuel (1994) and related issues of the nonlinear dynamics of upscale transfer are addressed by Thorpe & Rotunno (1989) for the dry problem. For this area of atmospheric mesoscale dynamics, the emphasis has mainly been on the effect of vertical shear and the so-called slantwise convection problem.

An unresolved issue in inertial instability is the problem of the vertical scale selection, which a linear instability framework cannot resolve, even in the presence of a realistic small vertical diffusion. Zonal asymmetries (Dunkerton 1983; Stevens & Cieselski 1986), as well as zonally localized shears and non-parallel flows have been studied (O'Sullivan & Hitchman 1992; Dunkerton 1993; Clark & Haynes 1996) in that respect within a hydrostatic framework.

Our approach here is based on a Taylor expansion of the absolute angular momentum of the flow in the vicinity of the neutral condition of instability, i.e. the basic states correspond to supercritical flows which are close to the marginal state of zero Ertel PV (§2). In §3 we make a short observational digression to provide evidence of nearly zero-Ertel PV in the time-mean subthermocline equatorial flow. We return to theoretical considerations in §4 to show that the geometry of the equatorial jets is best understood in terms of two parameters which combine the effects of latitudinal shear, latitudinal curvature of the flow and vertical shear. The two parameters are (i) the latitude of the dynamical equator, and (ii) a pseudo-Richardson number. The nonlinear equilibration regime of zonally symmetric latitudinal shear flows is then studied through non-hydrostatic numerical simulations in §5. The two first flow regimes correspond respectively to a stationary and a Hopf bifurcation and the energetics of their equilibration are detailed in §5.1. The role of large-scale damping is described in §5.2. The analogy between the nonlinear normal forms of the equatorial inertial

instability problem and the stratified Couette–Taylor (CT) problem is illustrated in §5.3, That subsection may be skipped by readers who are more interested by the geophysical application of inertial instability. Section 5.4 addresses the issue of the vertical selection problem. Finally, we explore in §6 the broader implications for the general circulation of the existence of regions of mean zero Ertel PV.

2. Generalized inertia of equatorial shear flows

We assume that both the basic state and secondary flows are zonally symmetric† and depend only on the meridional and vertical positions y and z. Such an assumption can be justified by the very long zonal scales of the equatorial deep jets (Ponte & Luyten 1989), and is appropriate for a first approach. Let $(\overline{u}(y,z),\ 0,0)$ and $\overline{\rho}(y,z)$ be the basic-state velocity and density fields. The vertical Coriolis parameter is $f = \beta y$ in the equatorial beta-plane approximation and geostrophic balance implies

$$\beta y \overline{u} + \frac{1}{\rho_0}\overline{p}_y = 0, \tag{2.1}$$

where $\overline{p}$ is the pressure field. The vertical momentum equation is

$$-\gamma \overline{u} + \frac{1}{\rho_0}\overline{p}_z = -\frac{g}{\rho_0}\overline{\rho}, \tag{2.2}$$

where $\gamma = 2\Omega$ is the horizontal Coriolis parameter, which is neglected in the traditional approximation (Phillips 1966) but is retained in the present work, in view of its quantitative importance in the oceanic observations which are detailed in §3. From (2.1) and (2.2) we find

$$\frac{g}{\rho_0}\overline{\rho}_y = \gamma \overline{u}_y + \beta y \overline{u}_z, \tag{2.3}$$

which expresses the thermal wind balance when both the vertical and horizontal components of the Earth rotation vector $\boldsymbol{\Omega}$ are retained.

Equations of motion for the velocity disturbances (u,v,w) and density are

$$\left.\begin{aligned}
\frac{\mathrm{d}}{\mathrm{d}t}u + v(\overline{u}_y - f) + w(\overline{u}_z + \gamma) &= 0, \\
\frac{\mathrm{d}}{\mathrm{d}t}v + fu + \frac{1}{\rho_0}p_y &= 0, \\
\frac{\mathrm{d}}{\mathrm{d}t}w - \gamma u + \frac{1}{\rho_0}p_z + \frac{g}{\rho_0}\rho &= 0, \\
\frac{\mathrm{d}}{\mathrm{d}t}\rho + v\overline{\rho}_y + w\overline{\rho}_z &= 0,
\end{aligned}\right\} \tag{2.4}$$

where $\mathrm{d}/\mathrm{d}t$ denotes the rate of change for a material element and will be made explicit below.

Let Ψ be a streamfunction for displacement in the meridional plane, so that

$$v = -\Psi_z, \quad w = \Psi_y \tag{2.5}$$

because of the incompressibility condition

$$v_y + w_z = 0.$$

---

† This assumption is at the origin of the terminology of symmetric instability which is often used in the atmospheric sciences for referring to inertial instability.

The advection operator is thus $d/dt = \partial/\partial t + J(\Psi,.)$, where J is the Jacobian, since $\bar{v} = \bar{w} = 0$, hence $\overline{\Psi} = 0$.

Eliminating the pressure disturbance p from (2.4), and a being the radius of the earth, we obtain the equations for the conservation of the total angular momentum with respect to the Earth axis of rotation

$$\tilde{M} = a\left(u + \bar{u} + \gamma z - \beta\tfrac{1}{2}y^2\right), \tag{2.6}$$

the zonal component $\omega_1 = \nabla^2\Psi$ of vorticity ω, and total density:

$$\left.\begin{aligned} \frac{d}{dt}\tilde{M} &= 0, \\ \frac{d}{dt}\nabla^2\Psi - f u_z - \gamma u_y + \frac{g}{\rho_0}\rho_y &= 0, \\ \frac{g}{\rho_0}\frac{d}{dt}\rho + v(f\bar{u}_z + \gamma\bar{u}_y) - w\overline{\mathcal{N}^2} &= 0, \end{aligned}\right\} \tag{2.7}$$

where $\overline{\mathcal{N}^2}(y,z) = -g\bar{\rho}_z/\rho_0$.

The second equation in (2.7) shows that the time tendency of zonal vorticity is forced by the thermal wind imbalance of the disturbances, and is hence consistent with our assumption that $\overline{\Psi} \equiv 0$ since the basic state verifies (2.3).

Linearizing equations (2.7) by replacing d/dt by $\partial/\partial t$ and eliminating u and ρ, we obtain the Eliassen–Sawyer equation (Eliassen 1951; Sawyer 1949) for the meridional streamfunction Ψ

$$\frac{\partial^2}{\partial t^2}\nabla^2\Psi + \mathcal{L}(\Psi) = 0, \tag{2.8}$$

where the operator $\mathcal{L}$ is

$$\mathcal{L} = \frac{\partial}{\partial z}\left(A\frac{\partial\Psi}{\partial z} + B\frac{\partial\Psi}{\partial y}\right) + \frac{\partial}{\partial y}\left(B\frac{\partial\Psi}{\partial z} + C\frac{\partial\Psi}{\partial y}\right), \tag{2.9}$$

and coefficients A, B, C are only functions of the mean shears and stratification

$$A = f(f - \bar{u}_y), \quad B = f(\gamma + \bar{u}_z), \quad C = \overline{\mathcal{N}^2} + \gamma(\gamma + \bar{u}_z).$$

Stevens (1983) has discussed an equation which is equivalent to (2.8) for the case of spherical geometry. One can physically interpret the operator $\mathcal{L}$ as expressing the generalized inertia of the basic state in the presence of mean shears and stratification. The symmetry of the cross-derivative terms in (2.9) implies that $\mathcal{L}$ is self-adjoint and this important property results from the thermal wind balance of the basic state (2.3). If one assumes a time dependence of the form

$$\Psi(y,z,t) = \exp(\sigma t)\hat{\Psi}(y,z),$$

where σ may be complex, the self-adjoint character of $\mathcal{L}$ implies that σ^2 is real. This can be checked by multiplying (2.9) by the complex conjugate Ψ^* and by integrating over the whole domain, assuming $\Psi = 0$ at the boundaries. This yields

$$\sigma^2\iint|\nabla\hat{\Psi}|^2 dy dz = \iint\left[A\left|\frac{\partial\hat{\Psi}}{\partial z}\right|^2 + B\left(\frac{\partial\hat{\Psi}^*}{\partial z}\frac{\partial\hat{\Psi}}{\partial y} + \frac{\partial\hat{\Psi}}{\partial z}\frac{\partial\hat{\Psi}^*}{\partial y}\right) + C\left|\frac{\partial\hat{\Psi}}{\partial y}\right|^2\right] dy dz.$$

The integrals on both sides of the equality being pure real numbers, this proves the above statement. The growth rate σ is thus either pure real or pure imaginary

and possible modes are either growing/decaying or purely oscillatory. The pure real character of σ for the growing solutions implies that they are endowed with a cellular instability character, by which structures grow in place and do not involve any propagation effect. Restating the above result more concisely, the symmetry of the generalized inertia operator $\mathscr{L}$, which is verified if the basic state complies with thermal wind balance, leads to the distinctive cellular character of inertial instability. This key property is also at the origin of the observed sequence of flow transitions in the Couette–Taylor problem (Chossat & Ioss 1994).

A necessary criterion for instability is that the operator $\mathscr{L}$ is hyperbolic (Ooyama 1966),

$$B^2 - AC \geqslant 0,$$

or

$$f(f - \bar{u}_y)\left[\overline{\mathscr{N}}^2 + \gamma(\gamma + \bar{u}_z)\right] - f^2(\gamma + \bar{u}_z)^2 \leqslant 0. \tag{2.10}$$

Introducing the Ertel potential vorticity of the basic state as

$$Q_E = -[2\boldsymbol{\Omega} + \boldsymbol{\omega}] \cdot \frac{g\,\boldsymbol{\nabla}\bar{\rho}}{\rho_0},$$

$$\frac{g\,\boldsymbol{\nabla}\bar{\rho}}{\rho_0} = (0, f\bar{u}_z + \gamma\bar{u}_y, -\overline{\mathscr{N}}^2),$$

so that

$$Q_E = (f - \bar{u}_y)\left[\overline{\mathscr{N}}^2 + \gamma(\gamma + \bar{u}_z)\right] - f(\gamma + \bar{u}_z)^2, \tag{2.11}$$

the instability condition (2.10) is thus identical to

$$fQ_E \leqslant 0. \tag{2.12}$$

This is the well-known condition for the inertial instability of a stratified flow (Hoskins 1974), which replaces the Rayleigh (1916) condition of an adverse angular momentum distribution in the case of a stratified fluid. The usual condition (2.12) thus remains valid even when one relaxes the traditional approximation and takes into account the horizontal component of the Earth rotation vector. For zonally symmetric flows, e.g. Stevens (1983), the expression for Ertel PV can also be rewritten as

$$Q_E = \frac{g}{a\,\rho_0}\,J(\overline{M}, \bar{\rho}).$$

This expression states that the inertial stability depends upon the angle between isopleths of angular momentum and isopycnals, and the neutral condition $fQ_E = 0$ is equivalent to saying that the angular momentum is uniform on density surfaces.

Oceanographic values of the buoyancy frequency $\overline{\mathscr{N}}$ are around 2×10^{-3} s^{-1} for the equatorial subthermocline, and around 10^{-2} s^{-1} in the equatorial upper stratosphere/lower mesosphere (Hitchman *et al.* 1987), so that $\overline{\mathscr{N}} \gg \gamma$ and dominates the quantity within square brackets in (2.11). In general, for $(f - \bar{u}_y) \neq 0$, the first expression in the right-hand side of (2.11) is much larger than $f(\gamma + \bar{u}_z)^2$, because of the very stable mean stratification of equatorial regions. However, for locations where the absolute vertical vorticity $(f - \bar{u}_y) \approx 0$, the second term can play a quantitatively significant role in the Ertel potential vorticity distribution.

The two classes of shear flow which can trigger inertial instability can be readily identified from an examination of the expression for Ertel potential vorticity which is given in (2.11).

The case $f(f - \bar{u}_y) < 0$ and $\bar{u}_z + \gamma = 0$ is the analogue of the usual barotropic inertial instability problem (Dunkerton 1981; Stevens 1983) when the traditional approximation is relaxed.

The case $\bar{u}_z + \gamma \neq 0$ and $f - \bar{u}_y = 0$ corresponds to slantwise convection instability (Emanuel 1994), in the special case where the small deviation from the marginal state $Q_E = 0$ is occurring only in the z-direction. In contradistinction, previous studies of slantwise convection had chosen basic states where both $\bar{u}_z + \gamma \neq 0$ and $f - \bar{u}_y \neq 0$, so that departures from the marginal state are more complex to study.

3. Evidence of nearly zero Ertel potential vorticity

At this point we want to present some observational evidence that the subthermocline equatorial mean circulation displays values of nearly zero Ertel PV away from the equatorial plane $y = 0$. For that purpose, we have replotted the same data as that of figure 1 in a different way. Figure 2(*a*) displays the depth profiles of mean zonal velocity for five different latitudes ranging from $-1°$ to $+1°$ of latitude. In the depth range from 300 to 1800 m, there are clearly two distinct scales in the vertical: a large-scale linear vertical shear, upon which the smaller vertical scale of the deep jets is superposed. We have plotted on the same figure a dashed line, which is defined by $\bar{u} = -\gamma z$, where $\gamma = 2\Omega$ is the horizontal Coriolis parameter defined in §2. The largest vertical scale of the time-mean zonal velocity field is thus close to a value which counteracts the effect of the horizontal non-traditional Coriolis parameter for depths ranging from 300 to 1800 m. This observation has led us to take into account this term in the derivation in §2 of the condition for inertial instability on an equatorial beta-plane. On the other hand, figure 2(*b*) displays the meridional profile of the mean zonal velocity at a given level (600 m). Within a band of $1.2°$ latitude, the observed mean flow closely follows the dashed parabola defined by $\bar{u} = \frac{1}{2}\beta y^2$, which counteracts the effect of the traditional vertical Coriolis parameter $f = \beta y$.

The implication of both figures 2(*a*) and 2(*b*) is that the largest scale of the mean flow below the thermocline (which lies above 250 m at this longitude of the middle Pacific), has adjusted itself so as to cancel almost completely the gradient of angular momentum which is induced by the solid Earth rotation, in both the y- and z-directions.

The time-mean flow therefore approaches a state of uniform angular momentum, zero Ertel PV limit, which is precisely the neutral condition for inertial instability, even when the traditional approximation is relaxed (§2). Furthermore, an order of magnitude for the latitudinal extent of the region of zero PV at a given depth can be derived as follows. If the boundary of the zero-PV region coincides with an isopleth of the absolute angular momentum induced by the solid Earth rotation, $M = \frac{1}{2}\beta y^2 - \gamma z$, when the non-traditional Coriolis term is taken into account, then at the vertical distance from the bottom of the zero-PV region of $\delta z = (1800 - 600) = 1200$ m, which corresponds to figure 2(*b*), the latitudinal width should be $\delta y = (2 \, a \, \delta z)^{1/2} \approx 124$ km , since $\gamma/\beta = a$. This value of δy is quite consistent with the latitudinal extent of $1.2°$ found in figure 2(*b*). Other levels of westward flows in the data set of figure 1 also display the same cancellation tendencies as in figure 2(*b*), with a general decrease of δy with δz, consistently with the above argument. The general relevance of these observations of zero Ertel PV to the general circulation of equatorial subthermocline regions remains however to be assessed from larger data sets. There are other instances of near-uniform angular momentum in y which have been reported for both the equatorial upper ocean (Gouriou & Toole 1993) and the tropical troposphere
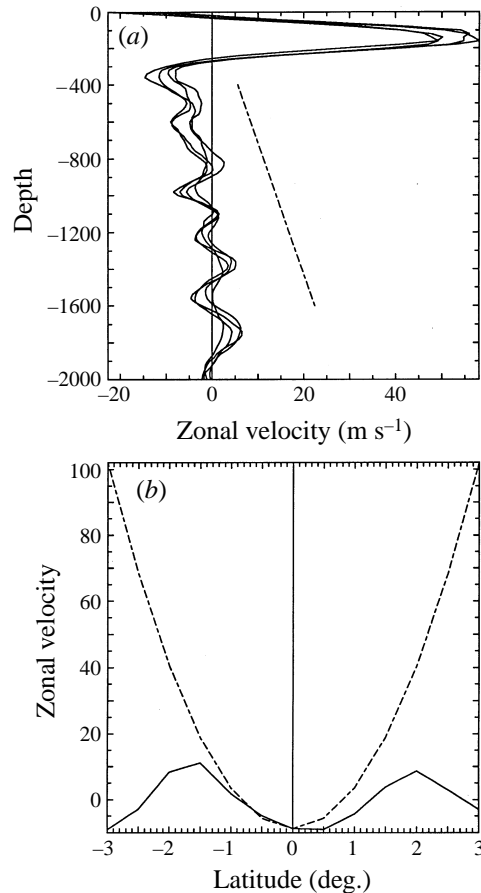
FIGURE 2. (*a*) Depth profiles of zonal time-mean velocity from PEQUOD at $-0.5°$, $0°$, $0.5°$, $1.0°$ latitude. The dashed line is defined by $\bar{u} = -\gamma z$. (*b*) Meridional profile of zonal time-mean velocity from PEQUOD at the 600 mlevel. The dashed parabola is defined by $\bar{u} = \frac{1}{2}\beta y^2$.

(Hoskins 1991), but the traditional approximation has been retained in these works, and no assessment of zero Ertel PV due to the γz-term contribution is performed.

In the absence of any mean flow, the main physical consequence of taking $\gamma \neq 0$ is the induced coupling of the barotropic and baroclinic free modes of motion, e.g. Miles (1974). The analytical difficulty which is caused by this coupling of the free modes may explain the wide usage of the traditional appproximation which has been made in the atmosphere-ocean literature. We have some observational evidence that the time-mean flow below the equatorial thermocline is close to $\bar{u}_z + \gamma = 0$, which will be shown in §4 to be the condition for decoupling the barotropic and baroclinic inertial modes. The decoupling of inertial modes can thus be retrieved locally even for $\gamma \neq 0$.

4. Simple inviscid hydrostatic solutions

We study here the two limiting cases mentioned at the end of §2 in order to gain some insight into which parameters govern the geometry of the stacking of the

secondary flow disturbances. We consider a basic state of the flow such that

$$\bar{u}(y, z) = u_0 + \epsilon y + \delta \tfrac{1}{2} y^2 + \bar{u}_z z. \tag{4.1}$$

Using the notation

$$A = \beta(\beta - \delta)y^2 - \epsilon\beta y,$$
$$\widetilde{\mathcal{N}}_0^2 = \widetilde{\mathcal{N}}^2 + \gamma(\gamma + \bar{u}_z),$$
$$\widetilde{u}_z = \bar{u}_z + \gamma,$$

the angular momentum of the basic state is

$$\overline{M} = a(u_0 + \epsilon y - (\beta - \delta)\tfrac{1}{2} y^2 + \widetilde{u}_z z). \tag{4.2}$$

For hydrostatic dynamics, the zonal vorticity reduces to $\omega_1 = \partial^2 \Psi / \partial z^2$, and the corresponding Eliassen–Sawyer equation (2.8) is

$$(\sigma^2 + A)\Psi_{zz} + \widetilde{\mathcal{N}}_0^2 \Psi_{yy} + 2\beta y \widetilde{u}_z \Psi_{yz} + \beta \widetilde{u}_z \Psi_z = 0, \tag{4.3}$$

where $\bar{u}_z$ is assumed constant as the stratification frequency $\widetilde{\mathcal{N}}_0^2$.

Introducing the new set of variables (y, ξ) with

$$\xi = z - \frac{\beta \widetilde{u}_z}{\widetilde{\mathcal{N}}_0^2} \frac{y^2}{2}, \tag{4.4}$$

we look for solutions of the form $\Psi = \check{\Psi}(y) \exp(ik\xi)$, where k is a pseudo-vertical wavenumber in the new set of variables (y, ξ).

Setting

$$\left.\begin{array}{l} y^* = (y - y_0)/\lambda, \quad y_0 = s\epsilon\beta/(2\beta_n^2), \quad \lambda^2 = \widetilde{\mathcal{N}}_0/(k\beta_n), \\ \beta_n = \beta|1 - 1/\widetilde{Ri}|^{1/2}, \quad s = \text{sign}\,(1 - 1/\widetilde{Ri}), \quad 1/\widetilde{Ri} = \widetilde{u}_z^2/\widetilde{\mathcal{N}}_0^2 + \delta/\beta, \end{array}\right\}. \tag{4.5}$$

equation (4.3) becomes

$$\check{\Psi}_{y^*y^*} - s\,y^{*2}\check{\Psi} = \frac{k}{\widetilde{\mathcal{N}}_0\beta_n}\left(\sigma^2 - s\beta_n^2 y_0^2\right)\check{\Psi}. \tag{4.6}$$

Following the sign of s the growing solutions ($\sigma^2 > 0$) to this differential equation will be either equatorially trapped or extra-equatorial, since the solutions will be of the Hermite-function type or of the parabolic-cylinder-function type. The parameter $\widetilde{Ri}$ is an effective Richardson number, in the presence of a meridional parabolic profile of the mean state, and the limit between equatorially trapped and extra-equatorial growing modes corresponds to $\widetilde{Ri} = 1$. The other relevant parameter is y_0 which is the new centre of symmetry of the solutions and has been named the dynamical equator by Stevens (1983), using a concept which had been originally introduced by Boyd (1978), in a study of the effects of a mean shear on equatorial waves.

4.1. *Equatorially trapped structures*

The solutions of Dunkerton (1981) and Stevens (1983) correspond to $s = 1$, $y_0 \neq 0$ in (4.6), and $\widetilde{u}_z \equiv 0$, i.e. the supercriticality is only due to the latitudinal shear of the basic state. The barotropic inertial problem, when formulated with the traditional approximation, has therefore the same mathematical structure as our present formulation which retains the horizontal component of the Coriolis force and moreover assumes $\bar{u}_z + \gamma = 0$. The streamfunction for overturning meridional motions
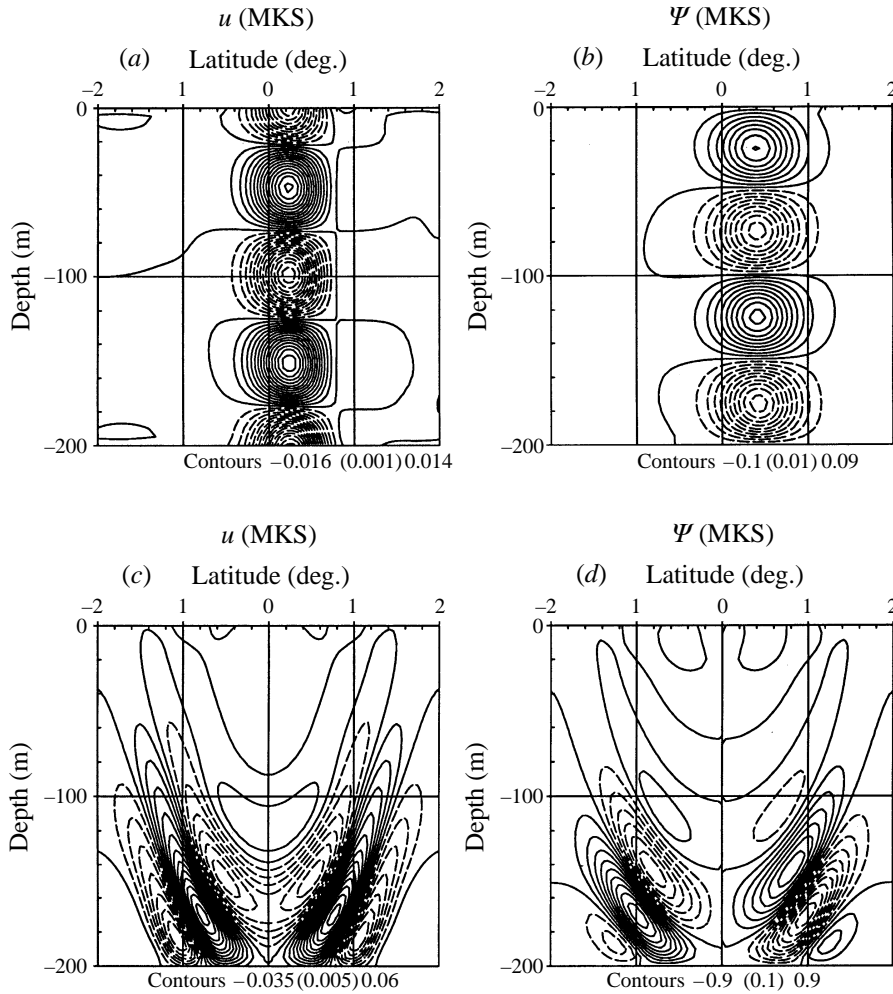
FIGURE 3. Most unstable mode for (*a*) zonal velocity perturbation $u(y, z)$ and (*b*) streamfunction $\Psi(y, z)$ for a latitudinal shear of the basic state. The same fields are shown respectively in (*c*) and (*d*) for a basic state defined by (4.14).

can be expressed as Hermite functions which are centred around the dynamical equator y_0:

$$\Psi \propto \exp(-\tfrac{1}{2}y^{*2})H_n(y^*),\qquad(4.7)$$

where $H_n(y^*)$ is the Hermite polynomial of order n. The growing modes are triggered by the existence of a latitudinal shear ($y_0 \neq 0$ for $\epsilon \neq 0$). The zonal velocity perturbation can be obtained from (2.4) and (2.5):

$$u = (\bar{u}_y - f)\frac{\partial \Psi}{\partial z} \propto \left(y^* - \frac{2y_0}{\lambda}\right)\exp(-\tfrac{1}{2}y^{*2})H_n(y^*).\qquad(4.8)$$

The velocity and streamfunction fields of these linearly unstable modes are illustrated in figures 3(*a*) and 3(*b*) respectively, for the case where the dynamical equator $y_0 = \epsilon/(2\beta) \approx 46\,\mathrm{km}$, for a vertical wavelength of $h = 100\,\mathrm{m}$ and for the gravest

latitudinal mode $n = 0$. All cases hereafter use $\beta = 2 \times 10^{-11}$ m^{-1} s^{-1} and $\widetilde{\mathcal{N}}_0 = 2 \times 10^{-3}$ s^{-1}.

The overturning motions are centred around $y = y_0$, while the zonal velocity is slightly more distorted latitudinally, and verifies $u = 0$ at $y = 2y_0$.

The inviscid solutions (4.7) cannot resolve the issue of the vertical scale selection problem, since their growth rate is

$$\sigma^2 = \beta_n^2 \, y_0^2 - (2n+1)\frac{\widetilde{\mathcal{N}}_0 \beta_n}{k} \tag{4.9}$$

(Stevens 1983). The growth rate increases with vertical wavenumber k, although it remains bounded by the upper limit $\sigma_{max} = |\beta_n \, y_0|$. Inertial instability is thus manifested most readily in the smallest vertical scales, and in the gravest ($n = 0$) latitudinal mode. This lack of a high-wavenumber cutoff in the growth rate is an intrinsic feature of the inviscid formulation of the centrifugal/inertial instability problem for both the unstratified and stratified case (Boubnov *et al.* 1995). Vertical diffusion needs to be invoked in order to regularize the problem at high wavenumbers (Dunkerton 1981).

On the other hand, an inviscid low-wavenumber cutoff can be computed from (4.9):

$$k_0 = \frac{4\beta_n \widetilde{\mathcal{N}}_0}{\epsilon^2} \, (1 - 1/\widetilde{Ri}), \tag{4.10}$$

which simplifies to

$$k_0 = \frac{4\beta \widetilde{\mathcal{N}}_0}{\epsilon^2} \, , \tag{4.11}$$

in the case where $\delta = \widetilde{u}_z = 0$. This inviscid lower bound can be interpreted geometrically by recognizing that the equatorial radius of deformation λ_0 which corresponds to k_0 is

$$\lambda_0 = \left[\frac{\widetilde{\mathcal{N}}_0}{\beta \, k_0} \right]^{1/2} = \frac{\epsilon}{2\beta} \equiv y_0,$$

and thus fits exactly between the geographical equator and the dynamical equator.

In summary, linear inviscid theory may explain the tendency for a preferred vertical stacking of small-aspect-ratio structures, which do not propagate. However, the vertical scales predicted by a linear framework are crucially dependent upon the specification of vertical diffusion. We shall see however in §5 that nonlinear advective effects induce an upscale transfer towards the reciprocal of the low-wavenumber cutoff (4.11). The analytical solution which has been detailed in this subsection may be relevant for the initial linear growth of the equatorial deep jets of figure 1.

4.2. *Extra-equatorial structures*

The solutions for $s = -1$ are parabolic cylinder functions and the streamfunction of secondary motions is

$$\Psi \; \propto \; H_o \left(\frac{k}{\widetilde{\mathcal{N}}_0 \beta_n} (\sigma^2 + \beta_n^2 y_0^2), \; y^* \right), \tag{4.12}$$

following the notations of Morse & Feschbach (1953, p. 1399) for the odd solution H_o versus y^*, and corresponds to eigenvalue $k(\sigma^2 + \beta_n^2 y_0^2)/(\widetilde{\mathcal{N}}_0 \beta_n)$.

We consider first the limiting case with $\epsilon \equiv y_0 \equiv 0$ and $f - \bar{u}_y = 0$, and $\tilde{u}_z \neq 0$, i.e. the supercriticality is only due to the vertical shear of the mean flow. A characteristic property of parabolic cylinder functions is that they become oscillatory away from $y^* = 0$ beyond a turning latitude defined by $y^* \approx 2(k\sigma^2/(\widetilde{\mathcal{N}}_0\beta_n))^{1/2}$. This result also holds for the zonal velocity perturbation which verifies

$$ u \propto \tilde{u}_z \frac{\partial \Psi}{\partial y}, $$

under the above simplifying assumptions. The zonal velocity perturbations, which are symmetric with respect to the geographical equator (since Ψ is odd), also become oscillatory away from the equator and reach their maximum away from the equator. In particular, the critical mode ($\sigma = 0$) corresponds to

$$ \left. \begin{aligned} \Psi &\propto (y^*)^{1/2} \, J_{1/4}(\tfrac{1}{2}y^{*2}), \\ u &\propto (y^*)^{3/2} \, J_{-3/4}(\tfrac{1}{2}y^{*2}), \end{aligned} \right\} \tag{4.13} $$

Solution (4.13) is such that the amplitude of the oscillations in u grows with y and is thus only valid in a latitudinally bounded domain, with a maximum amplitude at the boundary. This limiting case clearly illustrates the extra-equatorial character of the solutions.

More generally, the linear unstable modes given by (4.12) have growth rates which are determined by the geometry of the boundaries of the unstable domain and have to be determined numerically. The growing modes in u and Ψ are illustrated in figures 3(c) and 3(d) for the case of a westward basic flow such that

$$ \bar{u}(y, z) = U_w \left(1 - \frac{\beta}{2|U_w|}y^2 \right) \left(1 - \frac{\bar{u}_z}{|U_w|}(z + h) \right), \quad U_w < 0. \tag{4.14} $$

Such a choice corresponds to $y_0 = 0$ and verifies $f - \bar{u}_y = 0$ at the bottom of the domain $z = -h$, and $\widetilde{Ri} = 1 + \tilde{u}_z/\widetilde{\mathcal{N}}_0^2 > 1$ at that depth. Figures 3(c) and 3(d) correspond to $U_w = -0.30$ m, $h = 200$ m and $\bar{u}_z = 1.5 \times 10^{-3}$ s^{-1}. The growing modes display a high degree of symmetry with respect to $y = 0$ and show a tendency for a meridional stacking of structures which is characteristic of slantwise convection.

Furthermore, for $\tilde{u}_z \neq 0$, and $s = -1$, the largest growth rates in (4.6) will correspond to the largest vertical structures. The linear modes (4.12) may be relevant for the initial growth of the extra-equatorial features of figure 1, which present larger vertical scales than the equatorially trapped deep jets. Such solutions have not yet been examined in the literature to our knowledge. Much more observational and theoretical work is needed for characterizing the extra-equatorial time-mean flow structure and choice (4.14) is an oversimplification of the westward flow beneath the equatorial undercurrent in figure 1.

Finally, since the only parameter which determines the nature of the differential equation (4.6) is $1/\widetilde{Ri} = \tilde{u}_z^2/\widetilde{\mathcal{N}}_0^2 + \delta/\beta$, the effect of a vertical shear ($\tilde{u}_z \neq 0$) is similar to the effect of a westard curvature of the basic state ($\delta > 0$), for triggering extra-equatorial solutions.

5. Finite-amplitude non-hydrostatic simulations

In the remainder of the paper, we shall address the case of a supercritical latitudinal shear with $\tilde{u}_z \equiv 0$, and leave for further investigation the issue of the case of supercritical vertical shear. The nonlinear equilibration is studied through numerical

simulations of non-hydrostatic viscous/diffusive flows in the presence of a prescribed unstable basic state. The initial-value problem which is integrated numerically is

$$
\left.\begin{aligned}
\frac{\mathrm{d}}{\mathrm{d}t}(\widetilde{M}) &= (\mathrm{D}_v - r)(\widetilde{M} - \overline{M}), \\
\frac{\mathrm{d}}{\mathrm{d}t}\nabla^2\Psi + fu_z + \gamma u_y - \frac{g}{\rho_0}\rho_y &= (\mathrm{D}_v - r)\nabla^2\Psi, \\
\frac{g}{\rho_0}\frac{\mathrm{d}}{\mathrm{d}t}\rho + v(f\overline{u}_z + \gamma\overline{u}_y) - w\overline{\mathcal{N}}^2 &\left(\frac{1}{Pr}\mathrm{D}_v - r\right)\rho.
\end{aligned}\right\}
\tag{5.1}
$$

Initial conditions correspond to small disturbances which are superposed on the basic state and the flow is forced by a relaxation of the dynamical variables $(\widetilde{M},\ \Psi,\ \rho)$ to the unstable basic state $(\overline{M}, 0, 0)$, which is an exact solution of system (5.1). The relaxation is performed through the operator $(\mathrm{D}_v - r)$, which acts both on the small scales, through the eddy viscosity operator D_v, and on the energy-containing scales, through a Rayleigh damping term, where the time scale r^{-1} is chosen such that $r \ll \sigma_{max}$, where σ_{max} is the maximum linear growth rate of the problem.

The operator D_v is assumed to be self-adjoint and such that $\iint \Psi^* \mathrm{D}_v(\nabla^2\Psi)\mathrm{d}y\mathrm{d}z$ is a real positive number, Ψ^* being the complex conjugate of Ψ. A detailed study of the role of the Prandtl number Pr for the stratified centrifugal/inertial instability problem is given in Hua *et al.* (1996) and we show there that below a critical Prandtl number Pr_c, such that $Pr_c > 1$, eigenvalues of the linear growing modes remain purely real. Since it is plausible that small-scale turbulence is responsible for the eddy viscosity and diffusivity in oceanic flows, we choose here $Pr = 1$, and thus preserve the self-adjoint character of the right-hand side of (5.1).

The eddy viscosity operator D_v is prescribed as

$$
\mathrm{D}_v = \left[v_z\frac{\partial^2}{\partial z^2} + v_y\frac{\partial^2}{\partial y^2}\right],
$$

where v_z and v_y are constant vertical and horizontal eddy viscosities. Our choice of $v_y/v_z \approx \pi\widetilde{\mathcal{N}}_0/(2\beta h)$ is based on the assumption that the horizontal scale is $\pi\lambda$, where λ is the equatorial radius of deformation $\lambda = (\widetilde{\mathcal{N}}_0 h/(2\pi\beta))^{1/2}$ which corresponds to the vertical wavelength h. This yields orders of magnitude of $v_y/v_z \approx 10^6$ for our applications. For flows with very small aspect ratios, anisotropic diffusivities in the vertical and horizontal directions have been commonly used since Bryan (1969) to produce convection-dominated flows, otherwise conduction effects can dominate the solution (Quon & Ghil 1995).

The influence of a damping term which only acts on the density field (Newtonian cooling) has been considered by Clark & Haynes (1994) within a linear framework. They show that such a choice introduces complex eigenvalues and moreover suppresses the lower bound k_0 (4.10) of the band of unstable vertical wavenumbers. In contradistinction, our choice of a Rayleigh damping which acts identically on all dynamical variables, preserves the self-adjoint property. We shall discuss in the next section its role in the nonlinear equilibration of the solutions.

The viscous Eliassen–Sawyer equation is

$$
\left[\frac{\partial}{\partial t} - (\mathrm{D}_v - r)\right]^2 \nabla^2\Psi + \mathscr{L}(\Psi) = 0.
\tag{5.2}
$$

We have seen in §3 that $\mathscr{L}(\Psi)$ is self-adjoint (e.g. $\iint \Psi^*\mathscr{L}(\Psi)\mathrm{d}y\mathrm{d}z$ is a real number), so that multiplying (5.2) by Ψ^*, integrating over the domain and subtracting the

complex-conjugate expression yields

$$(\sigma - \sigma^*) \left[(\sigma + \sigma^*) \iint |\nabla \Psi|^2 \mathrm{d}y \mathrm{d}z + 2 \iint \Psi^* \mathrm{D}_v (\nabla^2 \Psi) \mathrm{d}y \mathrm{d}z \right] = 0. \qquad (5.3)$$

Growing modes correspond to $(\sigma + \sigma^*) > 0$, so that the term within square brackets is always positive and equation (5.3) implies that $\sigma = \sigma^*$ and the cellular character of the linear instability is preserved.

Boundary conditions are periodic in the vertical, while in the meridional direction Dirichlet boundary conditions are prescribed for u, Ψ, and no-flux conditions are prescribed for ρ (see Thorpe & Rotunno 1989 for a discussion of the physical meaning of the boundary conditions in the symmetric instability context).

5.1. *Nonlinear equilibration*

We have performed a numerical integration of system (5.1), with the same parameters as those used for the linear solutions of figures 3(a) and 3(b), e.g. $y_0 \approx \delta u / (2L\beta)$ is about 46 km and the maximal inviscid growth rate $\sigma_{max} = \beta y_0 \approx 0.92 \times 10^{-6} \mathrm{s}^{-1}$. The vertical eddy viscosity $v_z = 0.5 \times 10^{-4} \mathrm{m}^2 \mathrm{s}^{-1}$ and $v_y / v_z = 1.5 \times 10^6$, and Rayleigh damping is chosen as $r = \frac{1}{4} \sigma_{max}$. The domain height is 200 m, the domain width is 300 km on each side of the equator. The non-hydrostatic model is initialized with the hydrostatic most unstable mode defined by (4.8).

The nonlinear adjustment of the flow is such that eastward jets migrate towards the geographical equator, while westward jets move slightly in the opposite direction. The equilibrated state for the perturbation in zonal velocity u is shown in figure 4(a), with eastward perturbations located on the geographic equator with finite-amplitude jets of about $6.5 \mathrm{cm} \mathrm{s}^{-1}$. In figure 4($d$), the time behaviour of the total zonal velocity at a given depth and for $y = 0$ provides evidence that the system undergoes a transition from a steady unstable basic state without zonal jets to another steady state with secondary flows. Figures 4(b) and 4(c) correspond respectively to the equilibrated fields for the overturning streamfunction Ψ and the perturbation in density. The circulation of the overturning cells is such that the vertical position of westward jets coincides with meridional outflow away from $y = 0$, while the vertical position of eastward jets coincides with meridional inflow towards the equator. The meridional migration of eastward and westward jets in opposite directions, with a resulting net offset in their final positions, corresponds to an effective mixing of absolute angular momentum $\widetilde{M}$ with latitude. This is the generic mechanism by which the centrifugal instability triggered by equatorial shear stabilizes the flow.

Total density $\rho + \bar{\rho}(y, z)$ is shown in figures 5(a) and 5(b) respectively for time $t = 0$ and for the final equilibrated state. Thermal wind balance (2.3), when taking into account the horizontal Coriolis component, implies that for $\bar{u}_z = -\gamma$, the mean isopycnal surfaces in figure 5(a) display both a curvature, and a meriodional offset with respect to $y = 0$. This meridional offset illustrates the coupling between the barotropic and barolinic components of the basic state when $\gamma \neq 0$ (e.g. Miles 1974). On the other hand, a comparison of figures 4(a) and 5(b) reveals that the inertial secondary jets have a sizable geostrophic component.

Initial and final fields of fQ_E are shown in figures 5(c) and 5(d). Initially, the anomalous PV region extends from $y = 0$ to $y \approx 78$ km , with a minimum of $-1.2 \times 10^{-12} \mathrm{s}^{-2}$, while in the final state tiny values of fQ_E are observed inside the overturning cells and large negative values have been expelled to their boundaries. These negative values are larger than the initial ones and this result is consistent with the proof given in Thorpe & Rotunno (1989) that Ertel PV cannot be conserved during
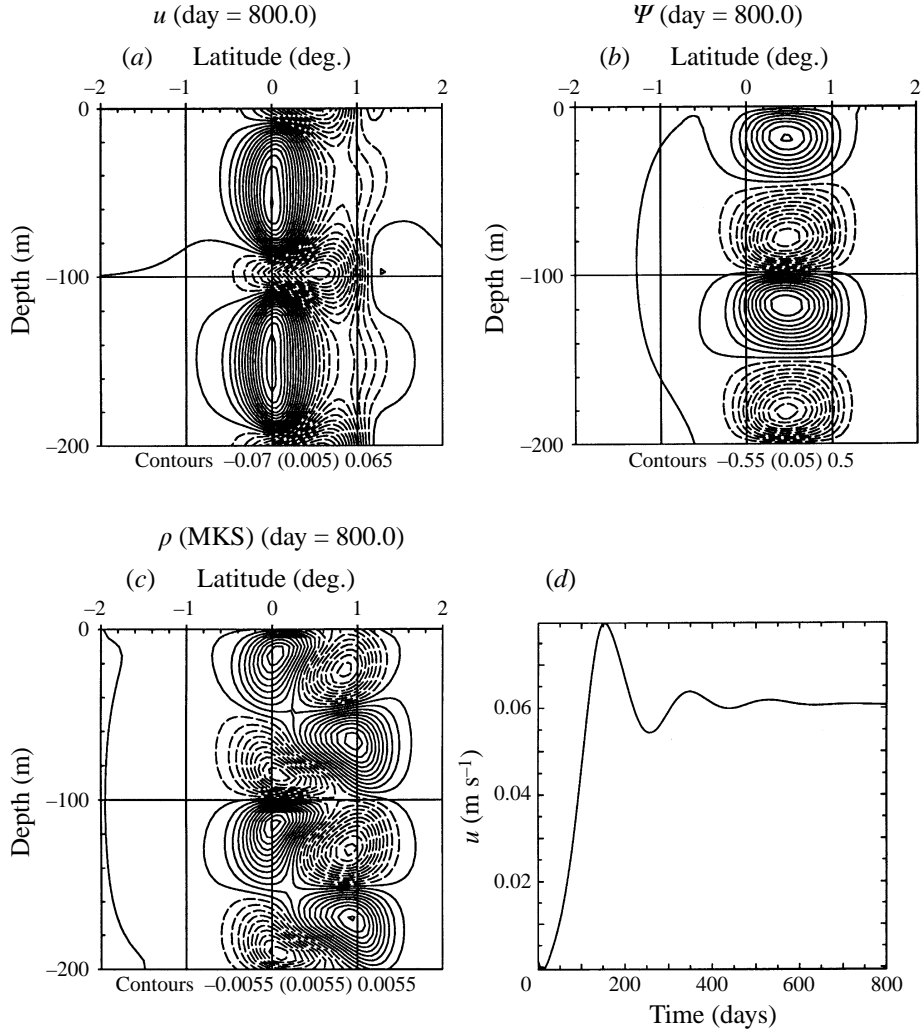
u (day = 800.0) Ψ (day = 800.0)

FIGURE 4. Case of a latitudinal shear of the basic state: equilibrated fields of perturbation fields for (a) $u(y,z)$, (b) $\Psi(y,z)$, and (c) $\rho(y,z)$; (d) time history of the zonal velocity pertubation u at a given point located at the equator.

the process of symmetric instability and that it can be fluxed countergradient because of nonlinarities. Therefore these dissipative cellular structures both redistribute and create negative PV values, with characteristics which are quite distinct from those of a simple downgradient mixing.

We have computed kinetic energy budgets, by multiplying the first two equations of system (5.1) by respectively u/a and Ψ, and by integrating over the whole domain. As expected, the driving is provided by the basic-state shear through $\iint u\, J(\Psi, \bar{u}) \mathrm{d}y\mathrm{d}z$, while the remaining terms act as sinks (the Coriolis and advective terms providing no net work). The energy gained from the basic shear is balanced primarily by Rayleigh damping and by the work against the background stratification within the overturning cells ($\iint \Psi g/\rho_0 \rho_y \mathrm{d}y\mathrm{d}z$), and vertical diffusion is three times more effective than horizontal diffusion as an energy sink, for our choice of v_z and v_y.

ρ (MKS) (day = 0)

(*a*) Latitude (deg.)

fQ_E (MKS) (day = 0)

(*c*) Latitude (deg.)

ρ (MKS) (day = 800.0)

(*b*) Latitude (deg.)

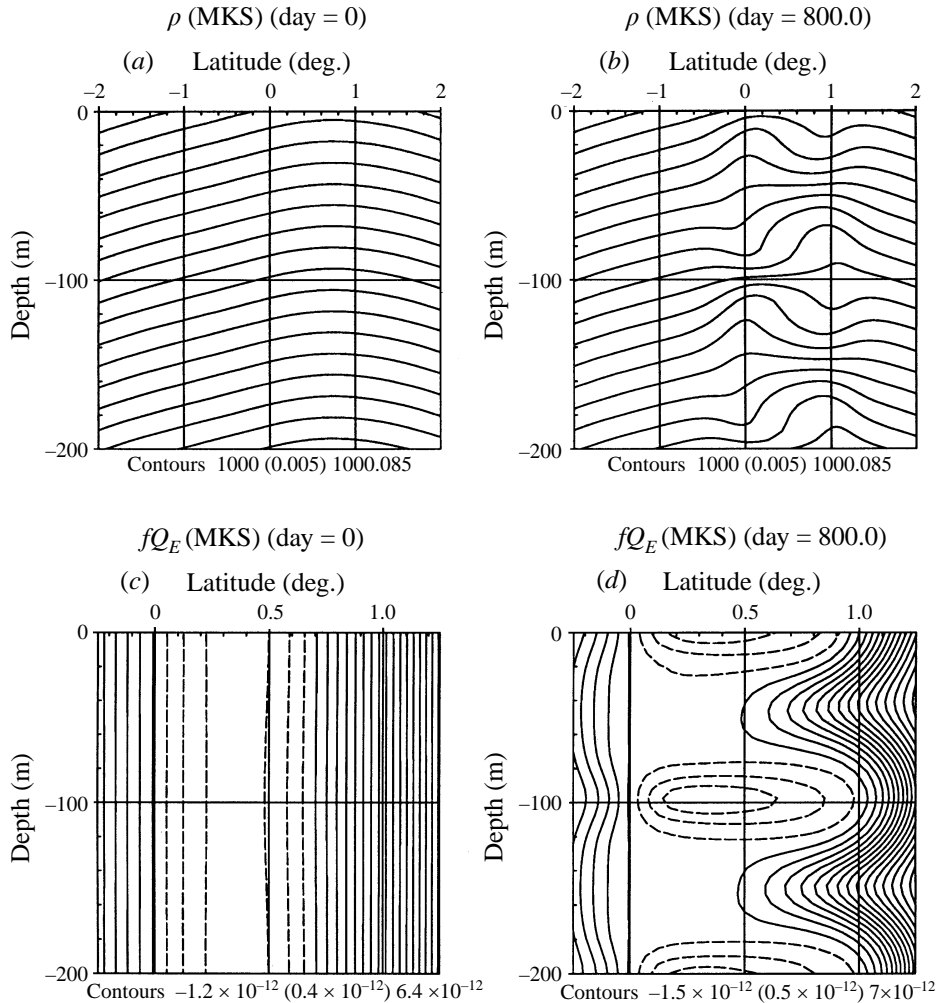fQ_E (MKS) (day = 800.0)

(*d*) Latitude (deg.)

FIGURE 5. Deviation of the total density field from ρ_0 for the same numerical simulation as figure 4: (*a*) at initial time; (*b*) in the equilibrated state. (*c*) and (*d*) Fields of $fQ_E/\widetilde{\mathcal{N}}_0$ respectively at the same times.

Nonlinear advection terms play an essential role in the equilibration of the structures of figures 4 and 5, since the linearized solutions of system (5.1) can only grow exponentially with time and therefore cannot equilibrate.

5.2. *Role of the large-scale damping*

In order to assess the role of the Rayleigh damping term in (5.1), we have performed another simulation, where we set the Rayleigh damping to zero, so that the only dissipation mechanism is acting at small scales through D_v. Parameters are in this case $v_z = 10^{-4}$, $v_y/v_z = 1.5 \times 10^6$, $r = 0$ for the sinks, while the domain geometry and mean shear remain the same as for the simulation of figures 4 and 5. Results are shown in figure 6(*a–d*) and the time series of figure 6(*d*) again corresponds to a transition from a steady-state flow to another steady-state flow after a very long transient oscillation which eventually decays. The final equilibrated fields of figure 6(*a–c*) reveal that the end state is a superposition of a barotropic latitudinal shear
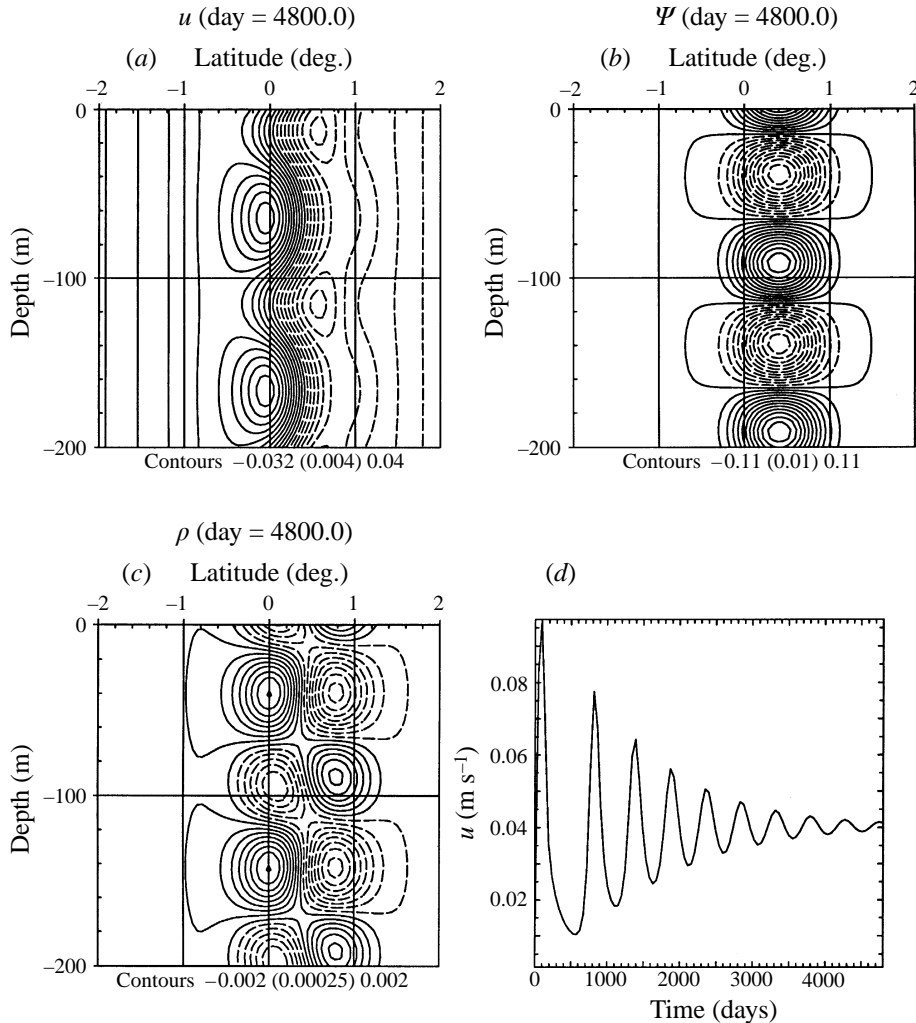
FIGURE 6. Case of a latitudinal shear of the basic state and for which the only sinks are the eddy viscous dissipation and diffusion. Equilibrated fields of (*a*) $u(y,z)$, (*b*) $\Psi(y,z)$, and (*c*) $\rho(y,z)$; (*d*) time history of total velocity field u at a point located at the equator.

flow and secondary overturning cells of weaker amplitude than in figure 4(*b*), but with identical vertical scales. It can be seen from figures 6(*d*) and 4(*d*) that the main effects of Rayleigh damping are first, to accelerate the transition between the initial steady state without jets to the steady state with jets, and secondly, to favour stronger jet amplitudes. The last result can be understood from considerations of energy balance, since the driving by the mean shear is compensated by the viscous work which is now acting both in the overturning cells and in the secondary barotropic latitudinal shear of figure 6(*a*). The transient behaviour in figure 6(*d*) corresponds to a decaying oscillation of the system between two configurations of the flow which are respectively a pure barotropic shear perturbation and pure secondary cellular motions. The final flow regime which is stationary is a mixture of these two configurations.
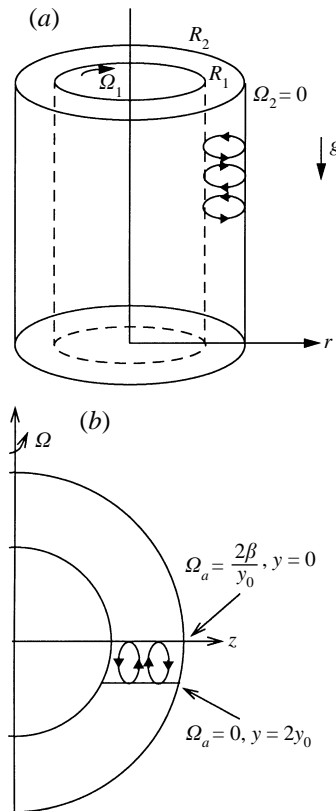
FIGURE 7. Set-up of the stratified Couette–Taylor experiment (*a*) and its analogy with the equatorial latitudinal shear problem (*b*).

5.3. *Analogy with the stratified Couette–Taylor problem*

The present subsection details the analogy between the equatorial inertial instability problem with latitudinal shear and the stratified Couette–Taylor (CT) problem. The existence of such an analogy immediately explains the preferred vertical stacking of the deep zonal jets (figure 7). This section may be skipped by readers who are more interested by the geophysical applications.

Equatorial regions are locations of maximum angular momentum of the planet and small deviations in the symmetries of the flow are likely to trigger centrifugal instabilities. Symmetry breaking is immediately induced by the existence of non-zero mean latitudinal shear at $y = 0$ and low-latitude regions are thus preferred locations for the occurrence of inertial instability. On the other hand, the CT problem, which concerns the flow between two concentric cylinders which can rotate independently, is the archetype of centrifugal instability.

For the homogeneous fluid problem, the transition from circular Couette flow to Taylor vortices can be understood in terms of Rayleigh's criterion, which states that the inviscid flow is linearly unstable if energy is liberated when two fluid rings of equal mass at radial distances r and $r + \mathrm{d}r$ are exchanged while conserving angular momentum. In particular, this condition is met if the mean angular momentum $\overline{M}(r)$ decreases outwards, as it does for any value of the inner cylinder rotation rate

($\Omega_1 \neq 0$), when the outer cylinder is fixed ($\Omega_2 = 0$) (see figure 7a). For finite viscosity, work is done in the exchange, hence $\overline{M}(r)$ reaches a finite gradient before the flow goes unstable. Taylor vortices mix the fluid in the interior of the flow, flattening the profile of $\overline{M}(r)$, which stabilizes the flow. Therefore in both the equatorial and CT problems we have the existence of a radial/latitudinal mean shear. Furthermore, the equatorial linear instability criterion $f\, Q_E < 0$ is satisfied within the latitudinal domain bounded by $y = 0$ (where the absolute vorticity $\Omega_a = f - \bar{u}_y = -\epsilon$), and by $y = 2\, y_0$ (where $\Omega_a = f - \bar{u}_y = 0$). The geographical equator $y = 0$ is thus the analogue of the rotating inner cylinder with $\Omega_1 \neq 0$, while the latitude $y = 2y_0$ is the analogue of the fixed outer cylinder where $\Omega_2 = 0$ (see figure 7b).† In order to have a valid analogy, we need furthermore the existence of a stable stratification in density in the axial direction of the concentric cylinders for the CT problem.

The general symmetries which are observed in the flows of wide-gap CT apparatus (Chossat & Ioss 1994) are also seen in the equatorial problem, namely that the flow remains invariant in a translation along the vertical/axial direction, in a reflection of $z \rightarrow -z$. This corresponds to

$$[u(y,z), v(y,z), w(y,z)] \rightarrow [u(y,-z), v(y,-z), -w(y,z)]$$

or equivalently for the zonally symmetric case to

$$[u, \Psi, \rho] \rightarrow [u, -\Psi, -\rho].$$

Finally, we have assumed zonal/azimuthal symmetry in this work. However, the analogy between the two systems is not exact because of the difference in the boundary conditions at the solid cylinders in Couette–Taylor flow and at the internal boundaries at the latitudes $y = 0$ and $y = 2y_0$.

A simulation for the stratified CT problem (figure 8a–d) has been performed for the case of a rotating inner cylinder and fixed outer cylinder, with radius ratio of $R_1/R_2 = 0.6$. Such a configuration corresponds to the same leading terms in the Taylor expansion of angular momentum $\overline{M}(r)$ with respect to $(r - R_1)$ as those of the equatorial problem (4.2). The stratification frequency is $\widetilde{\mathcal{N}}_0 = 1 \text{ s}^{-1}$ and we have set $Pr = 1$. The laboratory experiments of Boubnov *et al.* (1995) have revealed that the main effect of an axial density stratification is to reduce the height of the Taylor vortices and to cause the formation of density layers of small aspect ratio. Three-dimensional numerical simulations of these experiments are reported in Hua *et al.* (1996), along with a detailed study of the Prandtl number effect. For the present subsection, the simulation has been performed with a two-dimensional version of a Navier–Stokes code in cylindrical coordinates (Verzicco & Orlandi 1995), in the presence of a stable axial stratification.

The linear growing modes in the stratified Couette flow case (not shown) are very similar to the linear modes of the equatorial problem which had been shown in figure 3(a,b). Furthermore, the nonlinear equilibration patterns of figure 7 display the same features as those of the equatorial solutions of figure 4. As the amplitudes of the solutions grow, the mixing of angular momentum induces a radial migration towards the inner cylinder ‡ of retrograde azimuthal velocity perturbations, which are superposed on the primary circular Couette flow. On the other hand, prograde velocity perturbations migrate to the other side to the middle of the gap. One can

---

† For $\epsilon > 0$, $\Omega_a < 0$ and thus corresponds to a negative angular velocity of the inner cylinder.
‡ The inner cylinder is assumed to rotate in the negative direction in figure 8, consistently with the previous footnote.
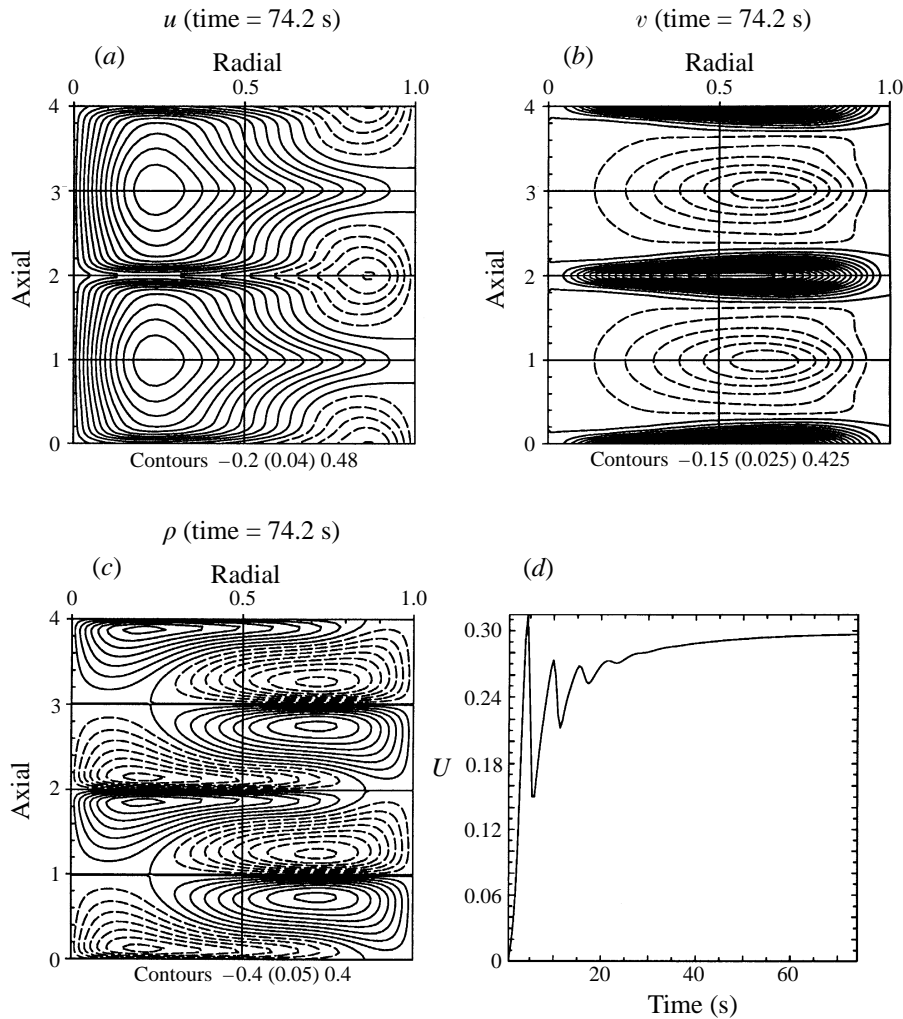
u (time = 74.2 s) v (time = 74.2 s)

FIGURE 8. Stratified Couette–Taylor simulation for a radius ratio of $R_1/R_2=0.6$ and a supercriticality of $Re/Re_c = 3$. Equilibrated fields of azimuthal velocity perturbation (a), radial velocity ($\propto \partial\Psi/\partial z$) ($b$), density pertubation; (c) time history of the total azimuthal velocity at a point located in the middle of the gap.

notice the difference in vertical extension of the prograde and retrograde flows which is also observed in figure 4(a). The equilibrated finite-amplitude perturbations in azimuthal velocity, are shown in figure 8(a). Figure 8(d) provides evidence that the stratified CT system has also undergone a stationary transition from one steady state to another steady state, which has secondary overturning cells (figure 8b). Therefore in both the equatorial inertial instability problem and in the stratified CT problem, zonal/azimuthal flows of opposite signs are offset in their meridional/radial positions in the nonlinearly equilibrated state. The radial velocity field in the stratified CT problem of figure 8(b) indicates the levels of radial outflow and inflow: analogously, the direction of the overturning cells in figure 4 is such that the westward jets correspond to 'outflow' away from the equator, while eastward jets correspond to

'inflow' towards the equator. As commonly observed in the CT apparatus (Tagg 1994), inflow levels are much broader than outflow ones.

The presence of layers can be seen in the density field perturbations (figures 8c and 4c) with a pinching of the isolines at given locations in the vertical. These mixing layers are very clearly diagnosed in the stratified experiments of Boubnov *et al.* (1995), through shadowgraph images which are sensitive to the second spatial derivative of density. This gradient expulsion of the density field is associated with the existence of the overturning cell motions of figure 8(b).

5.4. *Vertical scale of inertial jets*

Questions of geophysical interest are what sets the vertical scale of the jets which are observed in figure 2(a), and can the result be predicted theoretically? In the presence of a small-scale turbulence which is parameterized by a second-order diffusion/viscosity, the scales which are selected at onset of instability have been shown by Dunkerton (1981) to be accurately retrieved by the approximation $\sigma \rightarrow \sigma + v_z k^2$ in (4.9). This leads to critical values of wavenumber and shear of

$$k_c = (\widetilde{\mathcal{N}}_0 \beta / 4 v_z^2)^{1/5}, \quad \epsilon_c = \sqrt{5}(2 v_z \widetilde{\mathcal{N}}_0^2 \beta^2)^{1/5}. \tag{5.4}$$

For a value of $v_z = 2 \times 10^{-4} \text{ m}^2 \text{ s}^{-1}$, this yields

$$k_c = (2\pi/131 \text{ m}), \quad \epsilon_c = 2.05 \times 10^{-6} \text{ s}^{-1}.$$

We have checked numerically that our values of v_y have little impact on the vertical scale selection, and that we need to take into account the effects of Rayleigh damping through the approximation $\sigma \rightarrow \sigma + v_z k^2 + r$ in equation (4.9). The critical parameters for $v_z = 2 \times 10^{-4} \text{ m}^2 \text{ s}^{-1}$, $r = 3 \times 10^{-7} \text{ s}^{-1}$ are found to be

$$k_c = (2\pi/148 \text{ m}), \quad \epsilon_c = 2.39 \times 10^{-6} \text{ s}^{-1}.$$

These linearly determined scales are corroborated by a direct numerical simulation with $\epsilon = 1.02\epsilon_c$, and for the same values of v_z and r as above. The zonal velocity field is displayed in figure 9(a), confirming a height scale of $h \approx 150 \text{ m}$ at onset of instability.

However, for larger values of the supercriticality ϵ/ϵ_c, the nonlinear terms induce an upscale transfer, which is a generic property of two-dimensional nonlinear advection, e.g. Thorpe & Rotunno (1989). This effect is illustrated in figure 9(b) for a case with $\epsilon/\epsilon_c = 1.13$ and the resulting scale $h \approx 200 \text{ m}$ is such that $k/k_c = 148/200 \approx (\epsilon_c/\epsilon)^{5/2}$. This height scale of the equilibrated state is smaller than the neutral scale defined by the reciprocal of the inviscid bound (4.11) and we have

$$k \approx \sqrt{2} k_0. \tag{5.5}$$

Overall, all our simulations which equilibrate to a stationary flow regime are consistent with (5.5).

For further increase of the supercriticality such that $\epsilon/\epsilon_c > 1.22$, the vertical scale of the secondary jets still increases, but the temporal behaviour of the equilibrated state changes to an oscillatory state. This is illustrated in figure 9(c) for a case with $\epsilon/\epsilon_c = 1.33$ with a height scale of $h \approx 300 \text{ m}$ and we still verify $k/k_c \approx (\epsilon_c/\epsilon)^{5/2}$. The oscillatory transition (e.g. figure 9d) corresponds to an interaction between different axial scales and a shear destabilization of the outflow jet can be observed (this corresponds to the higher-frequency signal in figure 9(d) and this is also seen in the numerical simulations of the stratified CT problem of Hua *et al.* 1986). This secondary Hopf bifurcation of the flow, which follows a primary stationary pitchfork bifurcation
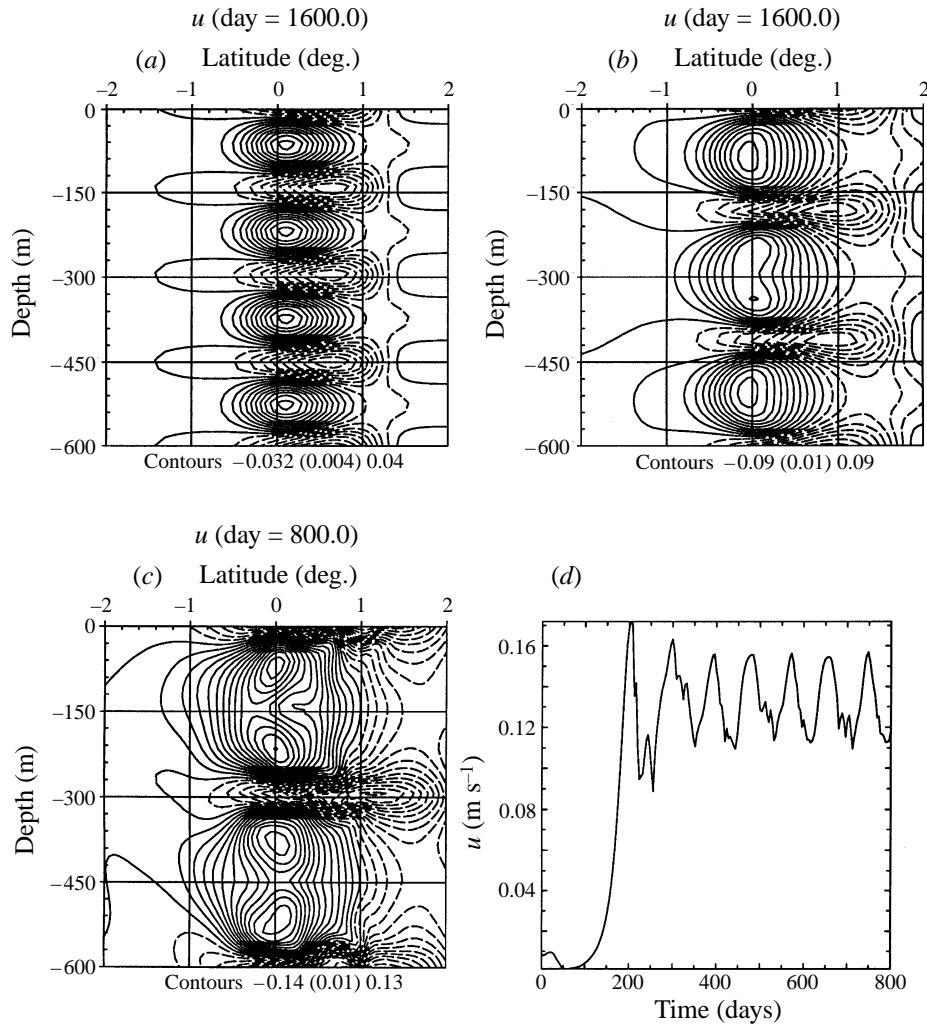
FIGURE 9. Zonal velocity fields at equilibration for basic states of supercriticality $\epsilon/\epsilon_c = 1.02, 1.16, 1.33$, respectively (*a*), (*b*), (*c*); the first two cases correspond to stationary flows while the last case is oscillatory; (*d*) time history of total zonal velocity field at a point located at the equator for a case with $\epsilon/\epsilon_c = 1.26$.

has also been observed by Zhao & Ghil (1991) in their study of nonlinear symmetric instability for a different set-up. The precise value of ϵ/ϵ_c for the secondary oscillatory transition is found to be dependent upon the height scale of the flow, and a more detailed study of the nature of the bifurcation diagram remains to be performed.

Overall, all our results are consistent with a dependence of the height scale such as

$$k_c/k \propto Re^{1/2}, \tag{5.6}$$

where the Reynolds number Re is defined as

$$Re = \frac{\epsilon^5}{v_z \beta^2 \widetilde{\mathcal{N}}_0^2}. \tag{5.7}$$

Such a definition of the Reynolds number is dimensionally consistent with both the

critical condition (5.4) of Dunkerton (1981) and with our result that $k/k_c \approx (\epsilon_c/\epsilon)^{5/2}$ at larger supercriticality. The adjunction of Rayleigh damping can be incorporated into the quantitative value of the critical Reynolds number at onset of instability, while the horizontal diffusion coefficient has little quantitative impact on the vertical scale selection. We note that the scale growth which is implied by (5.6) is commonly observed in convective systems (e.g. Koshmieder 1993).

For geophysical applications, the relevance of the second-order diffusion and Rayleigh damping parameterization which have been used in this study may be questionable. It is more likely that the eddy diffusion, rather than being externally prescribed, should instead be the result of the ongoing existing inertial instability and is therefore an integral part of its stabilizing mechanism (see the detailed discussion in Dunkerton 1981 and Hitchmann *et al.* 1987). An important result however is that the equilibration of the secondary jets is strongly dependent on the existence of a damping mechanism which can act effectively upon the largest scales in contrast with the second-order diffusion, and such a mechanism is represented here by the Rayleigh damping term.

6. Discussion

An analysis of the observed distribution of the mean angular momentum of subthermocline flow leads us to take full account of the non-traditional component of the Coriolis force, as was originally studied by Bretherton (1964). Other recent studies which have relaxed the traditional approximation are Colin de Verdière & Schopp (1995), and White and Bromley (1995). This term provides an inviscid upper bound for the latitudinal extent of the equatorial region which is susceptible to approach a zero-potential-vorticity state. This corresponds to a maximum of about 3° for the equatorial ocean.

Other observations in the equatorial regions of both the upper ocean (Gouriou & Toole 1993) and troposphere (Sardeshmukh & Hoskins 1985) have also been found to approach zero potential vorticity.

The *raison d'être* of near-zero Ertel PV values is to allow for transfer of asymmetries in angular momentum between the two hemispheres and inertial deep jets are the byproduct of this angular momentum mixing. We remark that this process may work in the interior of ocean basins, away from meridional boundaries and its existence has quite different dynamical implications from those of a single critical line at the equator. More work for determining the extension of tiny-PV regions in both the equatorial atmosphere, e.g. figure 3(*a*) of Hoskins (1991), and oceans is needed, while present observations on other planets like Venus suggest an extension of the zero-Ertel-PV region up to about 55°, e.g. Alisson, Del Genio & Zhou (1994). Further discussions of potential vorticity modelling of convectively driven axisymmetric circulations within tropical regions can be found in Schubert *et al.* (1991).

We have shown that a horizontal shear leads to a vertical stacking of finite-amplitude secondary flows (equatorially trapped jets), while a vertical shear leads to a meridional stacking of secondary flows (extra-equatorial jets). The final equilibrated state corresponds to eastward jets located on the geographic equator, while westward jets are located near the dynamical equator. Such a redistribution of zonal flows amounts to a mixing of absolute angular momentum. A closer examination of the observed *in situ* mean flow of figure 1 reveals indeed that, as already noted by Firing (1987), eastward flows appear to be closer to the geographical equator than westard jets which are further north, closer to the dynamical equator at about 0.6° latitude.

Finally, Firing also observes in the time series of zonal flow that transitions of the flow regime are smooth between states without deep jets and states with their presence and they do not seem to involve propagation effects. The vertical jets appear to grow in place. This observation is consistent with the present work which shows that the inertial instability problem, with our choice of parameterization of sinks, has the character of a cellular instability, with secondary flows growing in place without propagation.

The problem of vertical scale selection, in order to explain the scale observed for the equatorial deep jets, is strongly influenced by the 'gap width' or meridional extent of the unstable region where $fQ_E < 0$. We have shown in §5 that, provided a stable stratification in the axial direction is taken into account, there is a close, albeit not complete, analogy between the equatorial latitudinal-shear flow and the stratified Couette–Taylor problem. While the gap width is unambiguously defined for the CT problem, a possible rationale, which is based on a gap width analogue for the equatorial problem, would be to select the vertical mode whose equatorial radius of deformation times $\sqrt{2}$ fits between the geographical and dynamical equators. A dynamical equator of 0.6° would correspond to an upper bound for vertical scale of around 300 m, for $\widetilde{\mathcal{N}}_0 = 2 \times 10^{-3}$ s^{-1} and $\beta = 2 \times 10^{-11}$ m s^{-1}. This value is consistent with observations in figure 2(*b*).

Our explanation which is based on inertial instability coincides with the explanation given in the equatorial middle atmosphere for explaining the pancake instabilities (Hitchman *et al.* 1987; Knox 1996), which have geometric characteristics very similar to the deep jets. While solsticial shear is invoked to be at the origin of the phenomenon in the middle atmosphere, the cause of the differences in angular momentum between the two hemispheres, which lead to a mean latitudinal shear, remains to be elucidated for the oceanographic case.

The present investigation, as a first step, has chosen the simplifying framework of a zonally symmetric description, the rationale being that the first transition in stratified centrifugal instability appears to be clearly axisymmetric. Such an approach has intrinsic shortcomings, among which is the impossibility of having eastward maxima right at the equator, i.e. a zonally symmetric model precludes super-rotation with our choice of sink parameterization and boundary conditions (Held & Hou 1980; Read 1986). In particular, although our mechanism can produce eastward zonal velocity perturbations, u, near the geographical equator, it will not produce a net eastward maximum there in $u + \bar{u}$. A side remark, however, is that there is no strong evidence in figure 2(*a*) of a super-rotation associated with the deep jets: clear-cut eastward flows appear in the data only at depths greater than 1300 m, while the small vertical oscillations in zonal velocity are already visible at depths of 300 m. Recent studies of inertial instability by Dunkerton (1993) and Clark & Haynes (1996) have relaxed the zonal-symmetry assumption and shown the existence of local modes of instability within regions of anomalous potential vorticity.

Although we have opted for a fully non-hydrostatic formulation in this paper, the aspect ratios of the flows under consideration are such that there is little quantitative difference between numerical hydrostatic and non-hydrostatic simulations in the range of values of dissipation parameters which we have used and for the primary stationary transition. Higher oscillatory transitions can differ quantitatively between the two formulations.

Finally, we have opted to 'decouple' the effects of the vertical shear and horizontal shear in the present study of equatorial inertial instability, and we leave to future

investigations a more detailed study of vertical shear, as well as the more complex situation where both types of shear are present.

REFERENCES

ALLISON, M., DEL GENIO, A. D. & ZHOU, W. 1994 Zero potential vorticity envelopes for the zonal-mean velocity of the Venus/Titan atmospheres. *J. Atmos. Sci.* **51**, 694–702.

BENNETTS, D. A. & HOSKINS, B. J. 1979 Conditional symmetric instability - a possible explanation for frontal rainbands. *Q. J. R. Met. Soc.* **105**, 945–962.

BOUBNOV, B. M., GLEDZER, E. & HOPFINGER, E. J. 1995 Stratified Circular Couette flow: instability and flow regimes. *J. Fluid Mech.* **292**, 333–358.

BOUBNOV, B. M., GLEDZER, E., HOPFINGER, E. J. & ORLANDI, P. 1996 Layer formation and transitions in stratified circular Couette flow. *Dyn. Atmos. Oceans* **23**, 139–153.

BOYD, J. P. 1978 The effects of latitudinal shear on equatorial waves. Part I: theory and methods. *J. Atmos. Sci.* **35**, 2236–2258.

BOYD, J. P. & CHRISTIDIS, Z. D. 1982 Low wavenumber instability on the equatorial beta-plane. *Geophys. Res. Lett.* **9**, 769–772.

BRETHERTON, F. 1964 Low frequency oscillations trapped near the equator. *Tellus* **16**, 181–185.

BRYAN, K. 1969 A numerical method for the study of the circulation of the world ocean. *J. Comput. Phys.* **4**, 347–376.

CHOSSAT, P. & IOSS, G. 1994 *The Couette-Taylor Problem.* Springer.

CLARK, P. D. & HAYNES, P. H. 1994 Equatorial inertial instability: effects of vertical finite differencing and radiative transfer. *J. Atmos. Sci.* **51**, 2101–2109.

CLARK, P. D. & HAYNES, P. H. 1996 Inertial instability on an asymmetric low-latitude flow. *Q. J. R. Met. Soc.* **122**, 151–182.

COLIN DE VERDIÈRE, A. & SCHOPP, R. 1995 Flows in a rotating spherical shell : the equatorial case. *J. Fluid Mech.* **276**, 233–260.

DUNKERTON, T. J. 1981 On the inertial stability of the equatorial middle atmosphere. *J. Atmos. Sci.* **38**, 2354–2364.

DUNKERTON, T. J. 1983 A nonsymmetric equatorial inertial instability. *J. Atmos. Sci.* **40**, 807–813.

DUNKERTON, T. J. 1993 Inertial instability of nonparallel flow on an equatorial β plane. *J. Atmos. Sci.* **50**, 2744–2758.

ELIASSEN, A. 1951 Slow thermally or frictionally controlled meridional circulation in a circular vortex. *Astrophysica Norvegia* **5**, 19–60.

EMANUEL, K. A. 1988 Observational evidence of slantwise convective adjustment. *Mon. Weath. Rev.* **116**, 1805–1816.

EMANUEL, K. A. 1994 *Atmospheric Convection.* Oxford University Press.

ERIKSEN, C. C. 1981 Deep currents and their interpretation as equatorial waves in the western Pacific ocean. *J. Phys. Oceanogr.* **11**, 48–70.

FIRING, E. 1987 Deep zonal currents in the central equatorial Pacific. *J. Mar. Res.* **45**, 791–812.

GENT, P. R. & LUYTEN, J. R. 1985 How much energy propagates vertically in the equatorial oceans? *J. Phys. Oceanogr.* **15**, 997–1007.

GOURIOU, Y. & TOOLE, J. 1993 Mean circulation of the upper layers of the Western Equatorial Pacific Ocean. *J. Geophys. Res.* **98**, 22495–22520.

HELD, I. M. & HOU, A. Y. 1980 Nonlinear axially symmetric circulations in a nearly inviscid atmosphere. *J. Atmos. Sci.* **37**, 515–533.

HITCHMAN, H. M., LEOVY, C. B., GILLE, J. C. & BAILEY, P. L. 1987 Quasi-stationary zonally asymmetric circulations in the equatorial lower mesosphere. *J. Atmos. Sci.* **44**, 2219–2236.

HOSKINS, B. J. 1974 The role of potential vorticity in symmetric stability and instability. *Q. J. R. Met. Soc.* 480–482.

HOSKINS, B. J. 1991 Towards a PV-θ view of the general circulation. *Tellus* **43 AB**, 27–35.

HUA, B. L., LE GENTIL, S. & ORLANDI, P. 1996 First bifurcations in circular Couette flow with axial stratification. *Phys. Fluids* (in press).

JONES, A. C. 1985 The transition to wavy Taylor vortices. *J. Fluid Mech.* **157**, 136–162.

KAWASE, M. 1987 Establishment of deep ocean circulation driven by deep-water production. *J. Phys. Oceanogr.* **17**, 2294–2317.

KNOX, J. A. 1996 A theoretical and observational study of inertial instability and nonlinear balance. PhD thesis, University of Wisconsin-Madison, Dept. of Atmospheric and Oceanic Sciences.

KOSHMIEDER, E. L. 1993 *Bénard cells and Taylor vortices*. Cambridge University Press.

LUYTEN, J. R. & SWALLOW, J. C. 1976 Equatorial undercurrents. *Deep-Sea Res.* **23**, 1005–1007.

McCREARY, J. P. 1984 Equatorial beams. *J. Mar. Res.* **42**, 395–430.

McCREARY, J. P. & LUKAS, R. 1986 The response of the equatorial ocean to a moving wind field. *J. Geophys. Res.* **91**, 11691–11705.

MILES, J. W. 1974 On Laplace's tidal equations. *J. Fluid Mech.* **66**, 241–260.

MORSE, P. M. & FESCHBACH, H. 1953 *Methods of Theoretical Physics*. McGraw-Hill.

OOYAMA, K. 1966 On the stability of the baroclinic circular vortex: a sufficient criterion for stability. *J. Atmos. Sci.* **23**, 43–53.

O'SULLIVAN, D. J. & HITCHMAN, M. H. 1992 Inertial instability and Rossby wave breaking in a numerical model. *J. Atmos. Sci.* **49**, 991–1002.

PONTE, R. M. 1988 Equatorial Kelvin waves embedded in mean flow, with application to the deep jets. *J. Geophys. Res.* **93**, 13941–13946.

PONTE, R. M. & LUYTEN, J. 1989 Analysis and interpretation of deep equatorial currents in the central Pacific. *J. Phys. Oceanogr.* **19**, 1025–1038.

QUON, C. & GHIL, M. 1995 Multiple equilibria and stable oscillations in thermosolutal convection at small aspect ratio. *J. Fluid Mech.* **291**, 33–56.

RAYLEIGH LORD 1916 On the dynamics of revolving fluids. *Proc. R. Soc. Lond.* A **93**, 148–154.

READ, P. L. 1986 Super-rotation and diffusion of axial angular momentum: II. A review of quasi-axisymmetric models of planetary atmosphere. *Q. J. R. Met. Soc.* **112**, 253–272.

SARDESHMUKH, P. D. & HOSKINS, B. J. 1985 Vorticity balances in the tropics during the 1982-1983 El-Niño-Southern Oscillation event. *Q. J. R. Met. Soc.* **105**, 945–962.

SAWYER, J. S. 1949 The significance of dynamics instability in atmospheric motions. *Q. J. R. Met. Soc.* **75**, 364–374.

SCHUBERT, W. H., CIESELSKI, P. E., STEVENS, D. E. & KUO. H. C. 1991 Potential vorticity modeling of the ITCZ and the Hadley Circulation. *J. Atmos. Sci.* **48**, 1493–1509.

STEVENS, D. 1983 On symmetric stability and instability of zonal mean flows near the equator. *J. Atmos. Sci.* **40**, 882–893.

STEVENS, D. & CIESELSKI, P. E. 1986 Inertial instability of horizontally sheared flow away from the equator. *J. Atmos. Sci.* **43**, 2845–2856.

TAGG, R. 1994 The Couette-Taylor problem. *NonLinear Sci. Today* **4**, 1–25.

TAYLOR, G. I. 1923 Stability of a viscous liquid contained between two rotating cylinders. *Phil. Trans. R. Soc. Lond.* A **223**, 289–343.

THORPE, A. J. & ROTUNNO, R. 1989 Nonlinear aspects of symmetric instability. *J. Atmos. Sci.* **46**, 1285–1299.

VERZICCO, R. & ORLANDI, P. 1996 A finite-difference scheme for three-dimensional incompressible flows in cylindrical coordinates. *J. Comput. Phys.* **123**, 402–474.

WANG, D., MOORE, D. W. & ROTHSTEIN, L. M. 1994 Exact solutions to Kawase's linear model of deep-ocean circulation. *J. Phys. Oceanogr.* **24**, 2188–2195.

WHITE, A. A. & BROMLEY, R. A. 1995 Dynamically constistent, quasi-hydrostatic equations for global models with a complete representation of the Coriolis force. *Q. J. R. Met. Soc.* **121**, 399–418.

WUNSCH, C. 1977 Response of an equatorial ocean to a periodic monsoon *J. Phys. Oceanogr.* **7**, 497–511.

ZHAO, J. X. & GHIL, M. 1991 Nonlinear symmetric instability and intra- seasonal oscillations in the tropical atmosphere. *J. Atmos. Sci.* **48**, 2552–2568.